Fractals, Vol. 23, No. 2 (2015) 1550004 (11 pages)

DOI: 10.1142/S0218348X15500048

World Scientific
www.worldscientific.com

FRACTALS WITH HYPERBOLIC SCATORS IN 1 + 2 DIMENSIONS

M. FERNÁNDEZ-GUASTI
Lab. de Óptica Cuántica, Depto. de Física
Universidad A. Metropolitana Iztapalapa
09340 México Ap. Postal. 55-534 D.F., Mexico
mfg@xanum.uam.mx

Received December 27, 2012
Accepted December 19, 2014
Published April 6, 2015

Abstract

A nondistributive scator algebra in $1 + 2$ dimensions is used to map the quadratic iteration. The hyperbolic numbers square bound set reveals a rich structure when taken into the three-dimensional (3D) hyperbolic scator space. Self-similar small copies of the larger set are obtained along the real axis. These self-similar sets are located at the same positions and have equivalent relative sizes as the small M-set copies found between the Myrberg-Feigenbaum (MF) point and -2 in the complex Mandelbrot set. Furthermore, these small copies are self similar 3D copies of the larger 3D bound set. The real roots of the respective polynomials exhibit basins of attraction in a 3D space. Slices of the 3D confined scator set, labeled $\mathbf{c2i0}\mathbb{E}_{+}^{1+2}$ $(s; x, y)$, are shown at different planes to give an approximate idea of the 3D objects highly complicated boundary.

Keywords: Fractals; Hypercomplex Numbers; 3D Hyperbolic Numbers; Real Scators; Quadratic Iteration; Mandelbrot Set.

1. INTRODUCTION

The quadratic iteration with hyperbolic numbers has been studied by several authors.[1,2] Numeric evaluation of the quadratic iteration for initial $z_0 = 0$ gives rise to a square centered at $-\frac{7}{8}$ with sides equal to $\frac{9}{4\sqrt{2}} \approx 1.591$. The square diagonals lie parallel to the real and hypercomplex axes. It has been shown that if the bound criterion for a hyperbolic number $a + b\,\hat{\mathbf{e}}$, $(\hat{\mathbf{e}} \cdot \hat{\mathbf{e}} = 1,\ \hat{\mathbf{e}} \notin \mathbb{R})$ is $a^2 \leq \varepsilon$ and $b^2 \leq \varepsilon$, the bound set is equal to a square.[3] This set is the counterpart of the Mandelbrot set for complex numbers but in two-dimensional (2D) hyperbolic geometry. The boundary for the hyperbolic set, is made up of four straight lines void of the complexity shown by the M-set. There are neither small-copies of the set nor a structure within the bound region as can be seen in Fig. 1. All points in the real axis interval $[-2, \frac{1}{4}]$ yield bound iterations. These points are common to both, the complex and the hyperbolic sets, since the reals are a subset in either case.

On the other hand, the sets obtained for arbitrary initial point z_0 give rise to rectangles.[3] These rectangles obtained for the hyperbolic case, are the twins of the filled in Julia sets K_c, for the quadratic iteration in the complex plane. It has been pointed out that if the bound criterion is established with the hyperbolic number magnitude $a^2 - b^2 \leq \varepsilon$, the confined set need not be rectangles.[4] Nonetheless, numeric evaluations using the hyperbolic number's magnitude $|z|^2 = a^2 - b^2$ still yield squares for the hyperbolic M-set and rectangular figures for the K_c sets. Pavlov *et al.*[5] have argued that this result is due to rounding errors introduced by the computing algorithms when dealing with the difference of very large numbers. Indeed, we must recall that divergent points grow very quickly as exemplified by Douady[6] for complex numbers: If the modulus of $|z_n|$ is greater than 2, the modulus after 12 iterations $|z_{n+12}|$, is greater than the ratio of the volume of the known universe to the volume of a proton. In Figs. 1(a) and 1(b), we show the numerical results for the hyperbolic M-set using these two "bailout" criteria. The bound set is identical in either case but the escape velocity contours are much richer in the calculations that estimate distance with the hyperbolic metric criterion.

In this communication, we introduce a 3D hypercomplex algebra that contains the hyperbolic $\mathbb{H}$ numbers when only two components are considered. The hyperbolic or real scator algebra product is associative and commutative provided that divisors of zero are excluded. However, the product does not distribute over addition but in some special cases. It is possible to establish well-defined rules for the quadratic mapping with real scator algebra. That is, the square and addition operations, although not bilinear, can be consistently constructed. Furthermore, an order parameter can be established so that a bound criterion can be employed. The bound set produced by scator numbers under the quadratic iteration mapping, exhibit small self-similar copies of the larger set. The boundary of the confined set has a rich structure. The contours of the iso-escape velocity sets also show rather elaborate patterns.

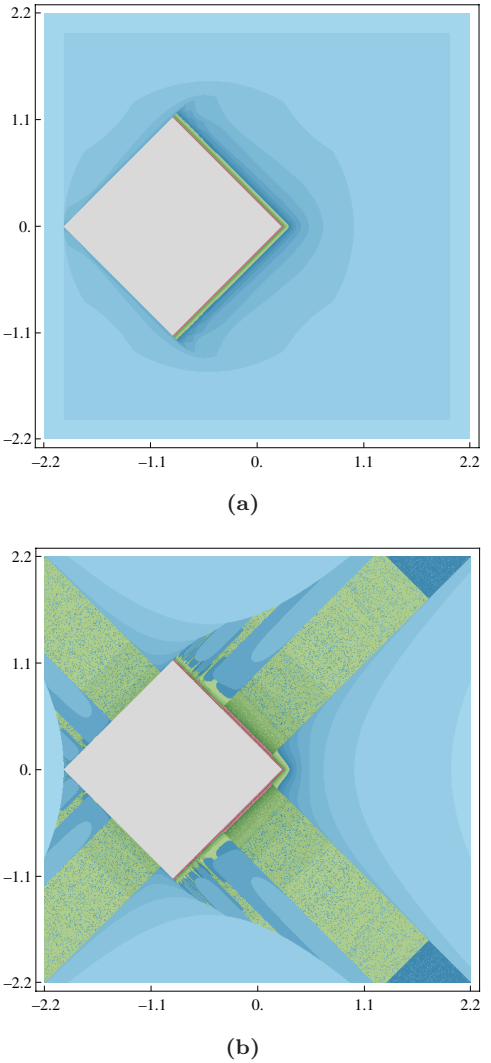

Fig. 1 Bound set (in light gray) under the quadratic iteration of hyperbolic numbers **c2i0**$\mathbb{H}$. The bound set is equal for both escape velocity criteria although the velocity maps are quite different (evaluation for each point is limited to 60 iterations). **(a)** Bounding condition is $a^2, b^2 \leq 4$ and **(b)** Bounding condition is $a^2 - b^2 \leq 4$.

2. HYPERBOLIC SCATORS

Hyperbolic or real scators are hypercomplex numbers that generate a nondistributive algebra in $1+m$ dimensions.[7] In $1+2$ dimensions (or higher dimensions), when a second hyperaxis is introduced, divisors of zero arise and there is no longer distributivity of the product over the sum. Real scator elements in 1+2 dimensions can be written as ordered triads in $\mathbb{R}^3$

$$\overset{o}{\varphi} = (F_0; F_1, F_2), \quad F_j \in \mathbb{R}.$$

The first component with subindex zero is labeled as the scalar component whereas subsequent components are termed the director components. Scator elements are labeled with an oval placed overhead.[a]

The *addition* operation for scators $\overset{o}{\alpha}, \overset{o}{\beta}$ is defined component-wise

$$\begin{aligned}\overset{o}{\alpha} + \overset{o}{\beta} &\equiv (A_0; A_1, A_2) + (B_0; B_1, B_2)\\ &= (A_0 + B_0; A_1 + B_1, A_2 + B_2).\end{aligned}$$

The scator set is a commutative group under the addition operation. The *product* or *multiplication* operation of two scators, $\overset{o}{\alpha} = (A_0; A_1, A_2)$ and $\overset{o}{\beta} = (B_0; B_1, B_2)$ is defined by $\overset{o}{\gamma} = \overset{o}{\alpha}\overset{o}{\beta} = (G_0; G_1, G_2)$, where the scalar component of the product is

$$G_0 = A_0B_0 + A_1B_1 + A_2B_2 + \frac{A_1B_1A_2B_2}{A_0B_0} \tag{2.1a}$$

and the director components of the product are

$$\begin{aligned}G_1 &= B_0A_1 + A_0B_1 + \frac{A_1A_2B_2}{A_0}\\ &\quad + \frac{A_2B_1B_2}{B_0},\end{aligned} \tag{2.1b}$$

$$\begin{aligned}G_2 &= B_0A_2 + A_0B_2 + \frac{A_1A_2B_1}{A_0}\\ &\quad + \frac{A_1B_1B_2}{B_0}.\end{aligned} \tag{2.1c}$$

In order to have a finite product, it is necessary that the scalar components are different from zero if two or more director components are different from zero in both factors

$$A_0, B_0 \neq 0 \text{ if } A_1B_1, A_2B_2 \neq 0. \tag{2.2}$$

This condition avoids divergences in the definitions of the scalar and director components. The subspace $\mathbb{E}_+^{1+2} \subseteq \mathbb{R}^3$, where the product is finite, is then

$$\begin{aligned}&(\mathbb{E}_+^{1+2}, \cdot)\\ &\quad = \{\overset{o}{\alpha}, \overset{o}{\beta} \in \mathbb{R}^3 : A_0, B_0 \neq 0 \text{ if } A_1B_1, A_2B_2 \neq 0\}.\end{aligned}$$

Hyperbolic 1+2-dimensional scators form a commutative group under the product operation provided that noninvertible elements and divisors of zero are excluded. Elements are invertible if $F_0 \neq F_1$, $F_0 \neq F_2$ and $F_0 \neq 0$ if any two director elements are different from zero. Furthermore, zero divisors of invertible elements are obtained if $A_1B_1 = -A_0B_0$ and $A_2B_2 = -A_0B_0$. The subspace $\mathbb{E}_g^{1+2}$ where the product satisfies commutative groupoid properties is

$$\begin{aligned}(\mathbb{E}_g^{1+2}, \cdot) = \Big\{&\overset{o}{\alpha}, \overset{o}{\beta} \in (\mathbb{E}_+^{1+2}, \cdot) : \overset{o}{\alpha}, \overset{o}{\beta} \neq 0,\\ &A_0 \neq A_k, B_0 \neq B_k, \frac{A_kB_k}{A_0B_0} \neq -1, k = 1, 2\Big\}.\end{aligned} \tag{2.3}$$

The *conjugate* of a scator $\overset{o}{\varphi} = (F_0; F_1, F_2)$ is defined by the negative of the director components while the scalar component remains unchanged

$$\overset{o}{\varphi}{}^* \equiv (F_0; -F_1, -F_2). \tag{2.4}$$

The square of the magnitude of a scator $\|\overset{o}{\varphi}\|^2$ is given by the scator times its conjugate,

$$\begin{aligned}\|\overset{o}{\varphi}\|^2 &= \overset{o}{\varphi}\overset{o}{\varphi}{}^*\\ &= \left(F_0^2 - F_1^2 - F_2^2 + \frac{F_1^2F_2^2}{F_0^2}; 0, 0\right).\end{aligned} \tag{2.5}$$

Notice that the special relativity metric is recovered for $F_0^2 \gg F_1^2, F_2^2$ if the scalar component is identified with time and the director components with two spatial axes. On these grounds, an alternative composition of velocities in a deformed Lorentz metric has been proposed using real scator algebra.[8] If condition (2.3) is fulfilled, the scator product of the magnitudes is equal to the magnitude of the scators product. This identity permits a generalization of Lagrange's identity. Furthermore, the scator magnitude product identity produces an infinite number of series identities.[9]

In $1+1$ dimensions, real scator algebra becomes identical to hyperbolic numbers algebra as may be readily seen from the product definition with any of the two director components with subindex 1 or 2 equal to zero. If we label the axes $(F_0; F_1, F_2)$ by s, $\hat{\mathbf{e}}_1$ and $\hat{\mathbf{e}}_2$, either plane $s, \hat{\mathbf{e}}_1$ or $s, \hat{\mathbf{e}}_2$ is identical to the hyperbolic number's plane.

[a] \overset{o} in LaTeX lore.

3. ITERATED QUADRATIC MAPPING

The quadratic mapping is given by

$$\overset{o}{\varphi} = \overset{o}{\varphi}{}_0^{\,2} + \overset{o}{c},$$

where the variable $\overset{o}{\varphi}$ and the constant $\overset{o}{c}$ are now scator elements. The iterated function satisfies the recurrence relationship

$$\overset{o}{\varphi}_{n+1} = \overset{o}{\varphi}_n^{\,2} + \overset{o}{c},$$

where the subindex stands for the iteration number. Julia sets in $\mathbb{E}_+^{1+2}$ are obtained by fixing $\overset{o}{c}$ and letting $\overset{o}{\varphi}_0$ vary in the real scator set $\mathbb{E}_+^{1+2}$. The points where the sequence $\overset{o}{\varphi}_n$ remains bounded comprise the filled in Julia set in $\mathbb{E}_+^{1+2}$. The Mandelbrot like set is obtained by fixing the initial point $\overset{o}{\varphi}_0 = (0;0,0)$ and varying the parameter $\overset{o}{c}$. Bound points obtained with the latter procedure comprise the corresponding M-set in $\mathbb{E}_+^{1+2}$. There are an infinite number of Julia sets on the complex plane. This number increases exponentially with dimension. Moreover, there are also many slices of the M-set in $\mathbb{E}_+^{1+2}$ compared with the unique sets obtained in $\mathbb{C}$ or $\mathbb{H}$. We propose the following notation to allow for some sort of orientation in this maze!

c2i **c**onfined {**2**} quadratic **i**terations, (that can be generalized to **cpi** for a pth power polynomial or p→ func for other *func*tion's mappings)

- Followed by **0** if the initial value of the variable is set to zero (parameter space) or $(F_0;F_1,F_2)$ if the initial constant is fixed to $(F_0;F_1,F_2)$ (dynamical space).
- Followed by the number set: $\mathbb{R}$ real, $\mathbb{C}$ complex, $\mathbb{H}$ hyperbolic, $\mathbb{E}_+^{1+m}$ real scator (in $1+m$ dimensions), etc.
- Followed, if necessary, by the plane $(D_0;D_1,D_2)$ that is being depicted.

Thus, the filled in Julia set in the complex plane K_c for the point $z = a + ib$ is the **c2i**$(a,b)\mathbb{C}$ set, whereas the Mandelbrot set in the complex plane is the **c2i0**$\mathbb{C}$ set. The K_c set for hyperbolic numbers is **c2i**$(a,b)\mathbb{H}$ set and the M-set is **c2i0**$\mathbb{H}$ set. This latter set is depicted in Fig. 1(b). The confined set is a square with smooth boundary. However, the layout of the escape values outside the set is already indicative of a richer structure. Since hyperbolic numbers are equivalent to scators with only one director component $\mathbb{H} \to \mathbb{E}_+^{1+1}$, the sets **c2i0**$\mathbb{H}$ and **c2i0**$\mathbb{E}_+^{1+1}$ are equal.[7]

The M-like set for real scators in $1+2$ dimensions, according with the proposed notation, is written as the **c2i0**$\mathbb{E}_+^{1+2}$ set. This set is no longer in two dimensions but in a 3D space. To commence its visualization, let us study "slices" or surfaces in the $s, \hat{\mathbf{e}}_1$ plane for constant $\hat{\mathbf{e}}_2$ component. Consider a constant scator with a very small hypercomplex constant in the second director component $\overset{o}{c} = (c_0; c_1, 10^{-17})$. The bound set, shown in Fig. 2, changes dramatically compared with the square (Fig. 1) observed when $F_2 = 0$. There is a rich structure within the square boundary.

Notation for low dimensional problems: When dealing with few dimensions it is simpler to label each component with a different letter and to allow for the subindex to represent the iteration number. In contrast, for the generalization to many dimensions, it is better to keep the subindex to label the component director elements.

The square of a scator is obtained from the product definition (2.1a)–(2.1c) with two equal scator factors. Let $\overset{o}{\beta} = \overset{o}{\alpha} = \overset{o}{\varphi} = (s;x,y)$, the scator squared is

$$\overset{o}{\varphi}{}^{2} = \left(s^2 + x^2 + y^2 + \frac{x^2y^2}{s^2}; \right.$$
$$\left. 2sx + \frac{2xy^2}{s}, 2sy + \frac{2yx^2}{s}\right). \qquad (3.1)$$

Recall that divisors of zero for invertible elements are obtained if the equalities $A_1B_1 = -A_0B_0$ and $A_2B_2 = -A_0B_0$ are fulfilled. For the quadratic mapping, these conditions are excluded, since for equal scators, they imply that $x^2 = -s^2$ and $y^2 = -s^2$. However, since s, x, y are real, the condition is never attained. Therefore, the only nonassociative elements come from noninvertible elements with $x^2 = s^2$ or $y^2 = s^2$.

On the other hand, distributivity of the product over addition does not hold. Consider the third iteration in terms of the initial value

$$\overset{o}{\varphi}_3 = \overset{o}{\varphi}_2^{\,2} + \overset{o}{c} = (\overset{o}{\varphi}_1^{\,2} + \overset{o}{c})^2 + \overset{o}{c}$$
$$= (\overset{o}{\varphi}_1^{\,2} + \overset{o}{c})(\overset{o}{\varphi}_1^{\,2} + \overset{o}{c}) + \overset{o}{c}. \qquad (3.2)$$

This scator is not equal to $\overset{o}{\varphi}{}'_3 = \overset{o}{\varphi}_1^{\,4} + 2\overset{o}{c}\overset{o}{\varphi}_1^{\,2} + \overset{o}{c}^{\,2} + \overset{o}{c}$. The numerical procedure evaluates the scator in each iteration and then proceeds to the next. Therefore, it produces sequences of the form described by Eq. (3.2). Notice that for hyperbolic numbers or scators with a single director component distributivity

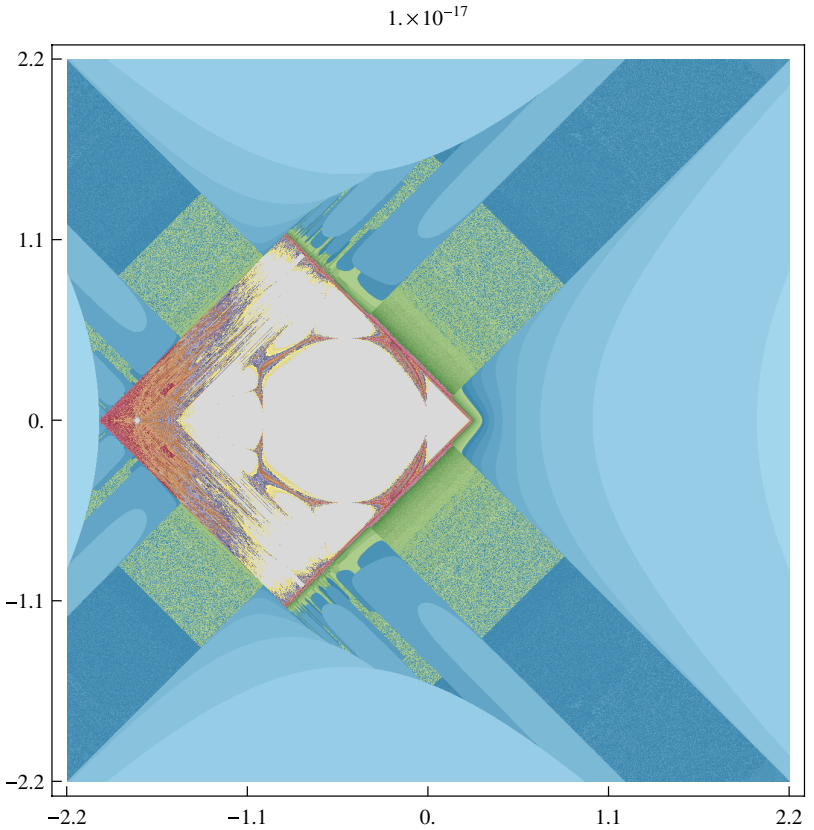

Fig. 2 **c2i0**$\mathbb{E}_{+}^{1+2}(c_0; c_1, 10^{-17})$ set (bound areas in light gray) under the quadratic iteration for real scators with second director equal to $F_2 = 10^{-17}$, limited to 60 iterations. The abscissa corresponds to the real or scalar s-axis where c_0 is plotted, while the ordinate corresponds to the first director component $\hat{\mathbf{e}}_1$ where c_1 is plotted ($\hat{\mathbf{e}}_x$ and x, respectively in the low dimension notation).

holds, $\overset{o}{\varphi}_2(s;0,y) = \overset{o\prime}{\varphi}_2(s;0,y)$ and either expression yields the same results.

Let us return to Fig. 2; it is symmetrical with respect to the hypercomplex ordinate axis $\hat{\mathbf{e}}_x$. Let us confirm that this is the expected result. The first two iterations starting with $\overset{o}{\varphi}_0 = (0;0,0)$ are $\overset{o}{\varphi}_1 = \overset{o}{c}$ and $\overset{o}{\varphi}_2 = \overset{o}{c}^2 + \overset{o}{c}$. The scator number squared plus the scator is

$$\begin{aligned}\overset{o}{\varphi}_2 &= (s_2; x_2, y_2)\\ &= \overset{o}{\varphi}_1^{\,2} + \overset{o}{\varphi}_1\\ &= \left(s^2 + x^2 + y^2 + \frac{x^2y^2}{s^2} + s;\right.\\ &\qquad \left. 2sx + \frac{2xy^2}{s} + x, 2sy + \frac{2yx^2}{s} + y\right). \quad (3.3)\end{aligned}$$

The resulting $\hat{\mathbf{e}}_x$ director component is $2sx + \frac{2xy^2}{s} + x$. This expression is an odd function of x, thus upon iteration, the function will be equal but with opposite sign under the transformation $x \to -x$. The bound criterion to establish the confined set is the squared magnitude $\|\overset{o}{\varphi}\|^2 = (s^2 - x^2 - y^2 + \frac{x^2y^2}{s^2}; 0, 0)$. This function is even under inversion of any of the axes. Therefore, the confined set, or the escape velocity iso-surfaces must be symmetric about the $\hat{\mathbf{e}}_x$ ordinate axis. An equivalent reasoning leads to symmetry about the $\hat{\mathbf{e}}_y$ axis. On the other hand, the bound set is asymmetrical with respect to the scalar (or real) s-axis. Indeed, from the above expression, the transformation $s \to -s$ does not have a well-defined parity for the resultant scalar term $s^2 + x^2 + y^2 + \frac{x^2y^2}{s^2} + s$. Thus, the iterated map will not be equal under inversion of the scalar axis. These symmetries can be extended by induction to the nth iteration. To summarize, the symmetries under inversion of the director axes are

$$\begin{aligned}s_n(s;x,y) &= s_n(s;-x,y)\\ &= s_n(s;x,-y),\\ x_n(s;-x,y) &= -x_n(s;x,y),\\ x_n(s;x,-y) &= x_n(s;x,y),\end{aligned}$$

$$y_n(s;x,-y) = -y_n(s;x,y),$$
$$y_n(s;-x,y) = y_n(s;x,y).$$

Symmetries under the director axes exchange are

$$s_n(s;x,y) = s_n(s;y,x),$$
$$x_n(s;x,y) = y_n(s;y,x),$$
$$y_n(s;x,y) = x_n(s;y,x).$$

There is therefore also symmetry with respect to the 45° planes in the director axes.

The bound set in Fig. 2 has an inner square on the right with a roundish center. Let us analyze this feature. If the scalar becomes small, all three components in iteration (3.3) become large for nonzero director components. Allow for y to be negligible in the scalar term second iteration; Impose the condition $s_2 \to 0$, so that the scalar term will produce a very large scator on the third iteration, $s^2 + x^2 + s = 0$. Notice that the s terms can be collected as $s^2 + s = (s + \frac{1}{2})^2 - \frac{1}{4}$. The equation is then $(s + \frac{1}{2})^2 + x^2 = \frac{1}{4}$, that is a circle of radius $\frac{1}{2}$ centered at $(-\frac{1}{2}; 0, 0)$. Therefore, the roundish rim feature where the set is unbounded is due to the scalar component becoming very small. It is of course not strictly a circle because the nonzero second director term has been neglected. This shape is distorted as the y plane is further away from the origin as can be seen in Fig. 5. The roundish center has two asymmetric triangular arrows on its sides. The point where the arrow on the right is joined to the main body is $s = 0$. The tip of this arrow is located at $s = \frac{1}{4}$ as expected from the real axis bound interval $[-2, \frac{1}{4}]$. The arrow on the left is in fact a sequence of smaller copies of the main body, a feature that is observed when the iteration limit is increased. The upper and lower symmetric structures blend with a ragged bound region inscribed in a larger square. The ragged boundary seems to split into a Fatou dust-like fractal. The scale in Fig. 2 has been maintained equal to that of Fig. 1(b) to show that the escape velocity contours remain fairly similar in either case. The coordinates s and x are scanned from -2.2 to 2.2 in both figures.

3.1. Self-Similarity — Small Copies

Let us have a closer look at the negative real scalar axis of the **c2i0**$\mathbb{E}_+^{1+2}(s;x,10^{-17})$ set in Fig. 3. It reveals smaller copies of itself! The pattern of the escape velocities in the vicinity of the set is quite complex. It exhibits straight bands at 45° whenever there is a copy of the larger set. Simultaneously

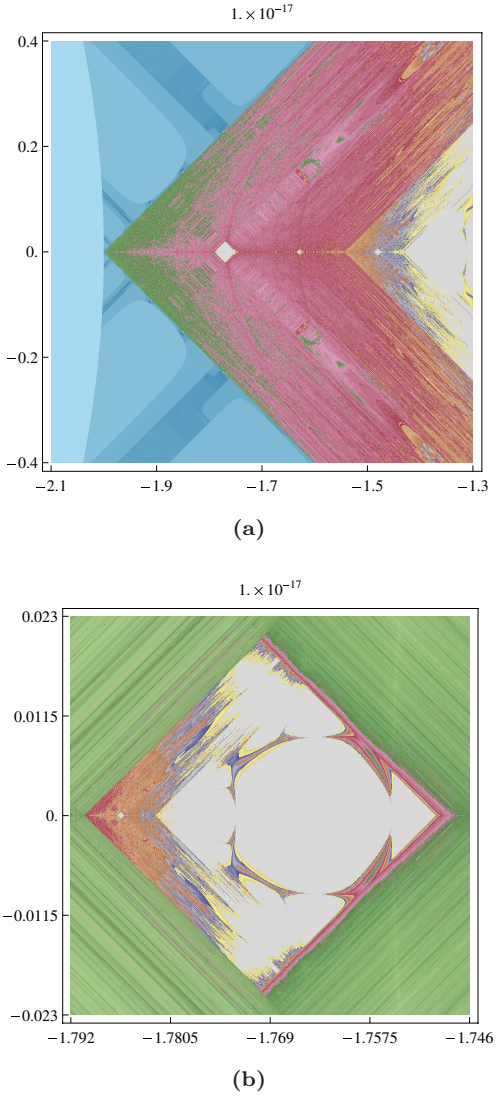

Fig. 3 Detail of the region between -2 and -1.3 on the left-hand side of the **c2i0**$\mathbb{E}_+^{1+2}(s;x,10^{-17})$ set shown in Fig. 2. Self-similar smaller copies with different sizes of the diamond-like figure are observed along the scalar axis! **(a)** Inset of Fig. 2 with magnification ×5.5, limited to 90 iterations and **(b)** Inset of Fig. 3(a) with magnification ×17.4 limited to 160 iterations (magnification ×95.6 of Fig. 2).

there are well-defined curves that resemble arcs of circles or parabolae in the midst of rather complicated structures. In Fig. 3(a), several small copies of the larger set are observed between -2 and -1.4. The copy centered at $-1.769\ldots$ is shown on a larger scale in Fig. 3(b). The number of iterations was increased as smaller regions are magnified, in order to preserve a similar resolution in the observed patterns. Its structure is remarkably similar to that of Fig. 2. It reproduces the roundish center with symmetric arrows on its sides and the symmetric structures above and below merging with a shred bound

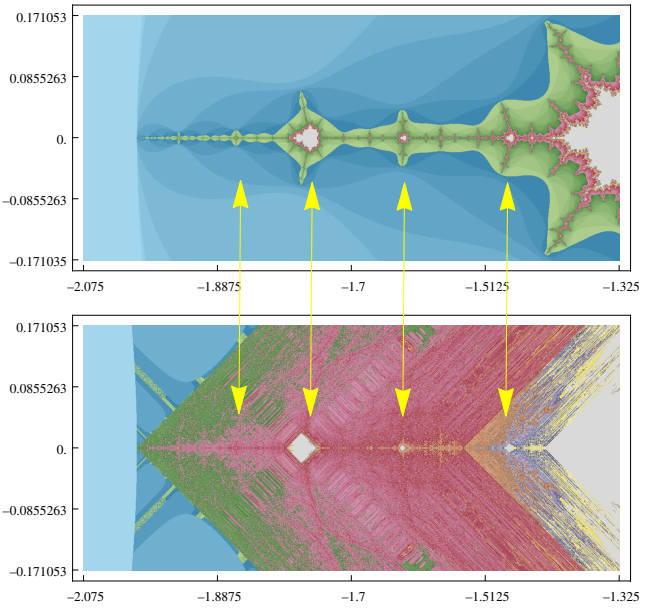

Fig. 4 Comparison between cardioïds in the vicinity of the real axis for the M-set and self-similar copies of the $\mathbf{c2i0}\mathbb{E}_{+}^{1+2}(s;x,10^{-17})$ scator set. The self-similar figures are located at exactly the same points (within computer error) on the real axis for either set.

region inscribed in a larger square. It also exhibits even smaller copies of itself at a much smaller scale in between -1.792 and -1.7805.

This result is of course reminiscent of the self copies of the M-set in the complex plane $\mathbf{c2i0}\mathbb{C}$. In Fig. 4, we compare the position of the on axis cardioïds with the self-similar copies of the $\mathbf{c2i0}\mathbb{E}_{+}^{1+2}(s;x,10^{-17})$ set. The cardioïds situated between the Myrberg-Feigenbaum (MF) point $-1.401\ldots$ and -2 of the complex Mandelbrot set,[10] are located at exactly the same positions on the real axis as the self-similar rhomboid-like figures of the $\mathbf{c2i0}\mathbb{E}_{+}^{1+2}(s;x,10^{-17})$ scator set within computer error. Furthermore, the relative size of the small cardïod-like components are proportional to the relative size of the rhomboid-like figures. For example, focus on the largest of these small copies located with its cusp at -1.75. This cusp corresponds to the right hand corner of the rhombus-like figure located at this very same point. As it is well known, there are an infinite number of small copies of the larger M-set. The $\mathbf{c2i0}\mathbb{E}_{+}^{1+2}$ set seems to also have an equivalent infinite number of small copies of itself in the vicinity of the scalar axis. Just as the M-set has a period doubling cascade region converging toward the MF point, there are an infinite number of smaller diamond-like figures in the scator set, apparently converging to this very same periodic-chaotic limit.

3.2. Planes with Constant Second Director Value

We have shown that a rich fractal-like structure is revealed if the second director component is set to a small value different from zero, (illustrated with $y = 10^{-17}$). In Fig. 5, we show a sequence of sets from $\mathbf{c2i0}\mathbb{E}_{+}^{1+2}(s;x,10^{-20})$ to $\mathbf{c2i0}\mathbb{E}_{+}^{1+2}(s;x,10^{-1})$. Each point is evaluated starting with $\overset{o}{\varphi}_0 = (0;0,0)$ and $\overset{o}{c} = (s;x,y)$, s is scanned from -2.125 to 0.375, while x is scanned from -1.25 to 1.25. The bound region becomes smaller and departs form the diamond-like shape, moving steadily toward a bird-like form as y is increased. The imprint is always squeezed in the forefront to the right in a plane

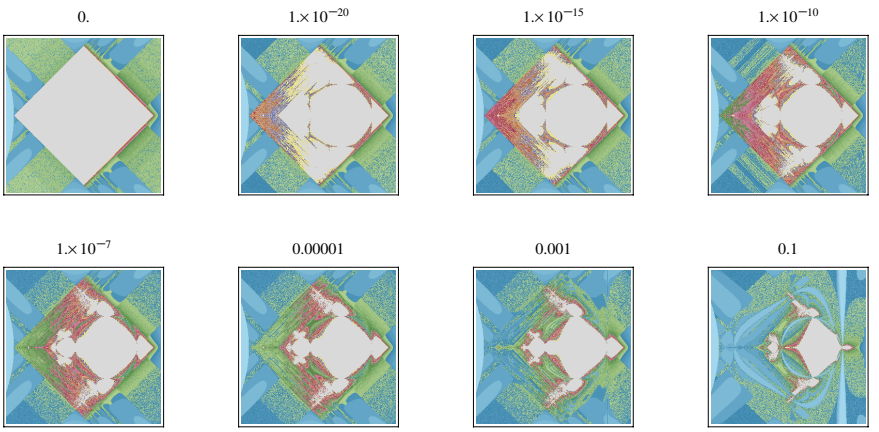

Fig. 5 Slices for small y values in the $s, \hat{\mathbf{e}}_x$ plane of the bound quadratic iteration $\mathbf{c2i0}\mathbb{E}_{+}^{1+2}(s;x,y)$ set with constant second director hypercomplex component y between 0 and 0.1 labeled on the upper border of each frame.

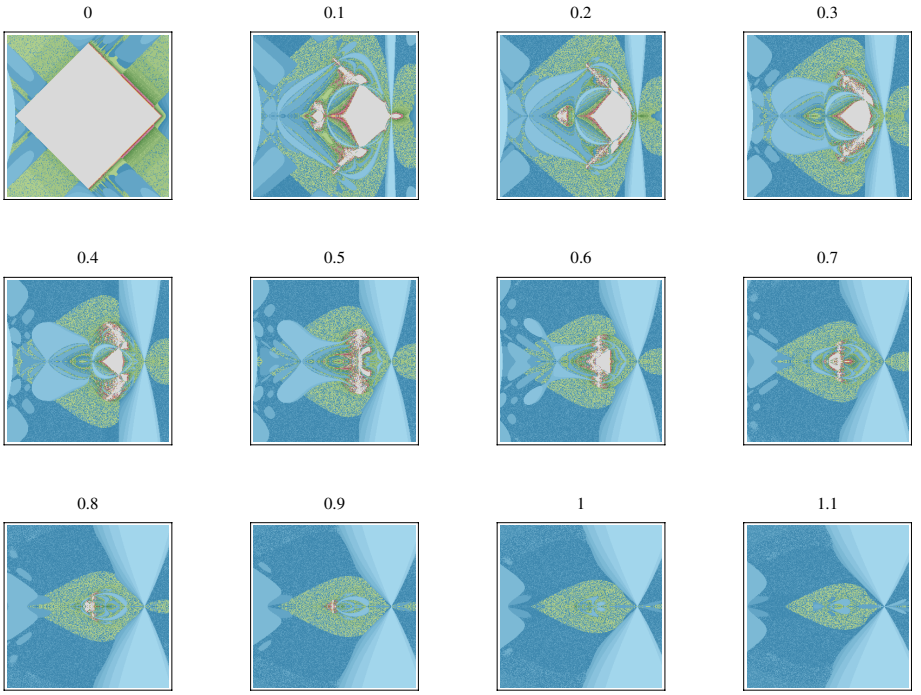

Fig. 6 Slices of the bound quadratic iteration **c2i0**$\mathbb{E}_{+}^{1+2}(s;x,y)$ set with the y hyper-axis between 0 and 1.1 in 0.1 steps. The abscissa s is scanned in the ± 1.25 interval centered at -0.875 whereas the ordinate x is scanned in the same interval but centered at the origin.

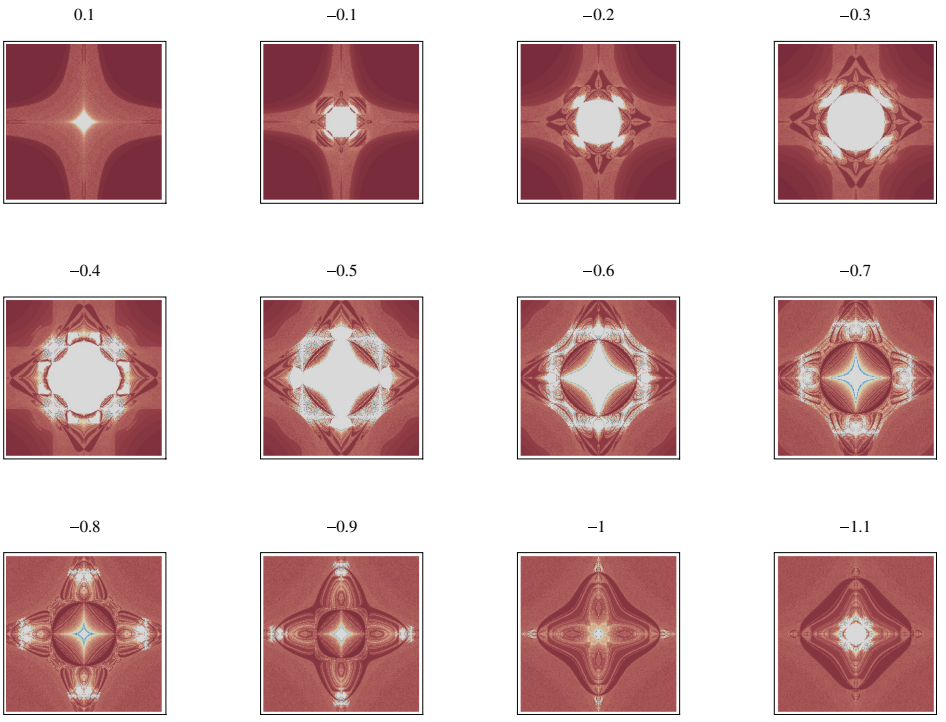

Fig. 7 Slices of the **c2i0**$\mathbb{E}_{+}^{1+2}(s;x,y)$ sets (in light gray) shown at constant scalar component s. The x,y hyperplane scans, where both axes represent hypercomplex components, span from -1 to 1 in both directions for all insets.

where $s = 0$. This result is expected because the scator magnitude (2.5) has a term $\frac{x^2y^2}{s^2}$ that diverges for nonzero x, y. Thus, no scator iteration can be bound in the region where this term becomes very large. The wings have a central lobe and possibly a second smaller lobe. They become fuzzy on the edge where a Fatou dust like boundary is observed. The arrow on the left side becomes a tail with three protuberances. The upper and lower bulges resemble smaller copies of the wings. The protuberance on the left is a copy of the larger protuberance, most likely with doubling period just as the buds in this region in the complex Mandelbrot set. Eventually, at $y = 0.1$, the tail is almost detached from the main body.

In another sequence, depicted in Fig. 6, we show sets from $\mathbf{c2i0}\mathbb{E}_+^{1+2}(s; x, 0)$ to $\mathbf{c2i0}\mathbb{E}_+^{1+2}(s; y, 1.1)$ in steps of $\triangle y = 0.1$. Again, points are evaluated in parameter space, s is scanned in the ± 1.25 interval centered at $-\frac{7}{8} = -0.875$, while x is centered at 0. The first and second insets in Fig. 6 correspond to the initial and final insets in Fig. 5. The bound set becomes smaller as the distance from $y = 0$ increases. There are no longer visible bound points at $y = 0.2$ for positive s (The bird looses its head). At $y = 0.3$, the remnants of the left arrow vanish and the bound region lies within the $(-0.875, 0)$ interval (The bird looses its tail). The out-most bound point must be located at $y = \frac{9}{8} = 1.125$, where the upper tip of the diamond is located. Recall that there must be a diamond-like shape in the perpendicular $s, \hat{\mathbf{e}}_y$ plane identical to the one shown in the first $s, \hat{\mathbf{e}}_x$ inset. This feature is not visible in the last inset of Fig. 6 because the tip becomes very thin and is thus difficult to see at this magnification. Indeed, from the sequence in Fig. 5, it can be seen that the tip is approximately 10^{-7} thick between 1.0 and 1.125.

4. THE x, y HYPERCOMPLEX — HYPERCOMPLEX PLANE

Consider planes where the scalar component s is maintained constant, while the values in x, y are scanned. These plots are entirely new since both axes are now hypercomplex axes. There is no real axis in these plots! Confined sets should be obtained, at least in the vicinity of $x = y = 0$, in the interval where s is between $[-2, \frac{1}{4}]$. In Fig. 7, $\mathbf{c2i0}\mathbb{E}_+^{1+2}(0.1; x, y)$ to $\mathbf{c2i0}\mathbb{E}_+^{1+2}(-1.1; x, y)$ sets are shown in steps of $\triangle s = 0.1$ for scans in x, y of ± 1. There are also confined sets images beyond

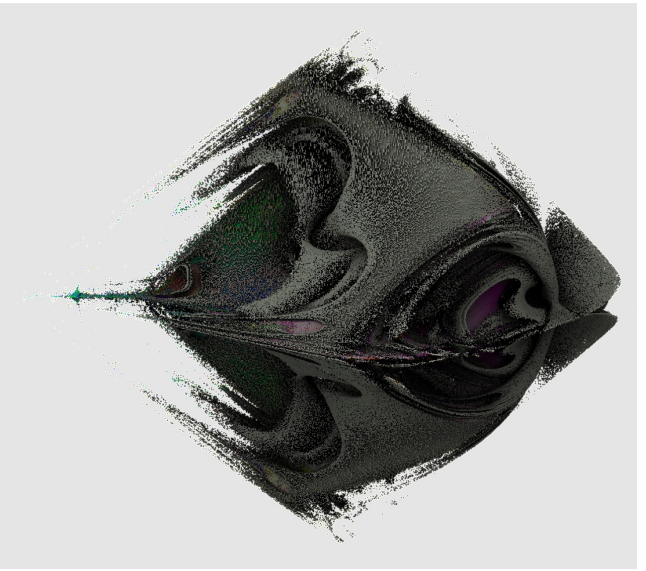

Fig. 8 3D rendering of the $\mathbf{c2i0}\mathbb{E}_+^{1+2}(s; x, y)$ set produced with P. Willenius rendering program.[11] The bud on the far left (in light blue) is a self similar copy of the larger set. The straight lines leading to vertices, sharper on the upper part and in perspective coming out of the page, correspond to the squares obtained for the planes $x = 0$ and $y = 0$.

$s = 1.1$ but with much smaller dimensions. The sets produced at x, y planes where self-similar copies were observed in the s, x plane, also exhibit self-similar structures in the x, y plane. The inversion symmetry as well as the additional 45° symmetry in the x, y plane in the director components described in the previous section, are observed in the numerical results depicted in Fig. 7. The ek[b]-like figure depicted at $s = 0.1$ is repeated at various planes, for example from -0.6 to -0.9. The four turbans in the diagonals of inset at $s = -0.2$ alternate with diploid figures on the axes lines. At $s = -0.4$ straight lines with fuzzy edges come out producing a square shape. In the following insets, remnants of the straight lines are displaced toward the edges until frame $s = -0.9$. At -1.0 an interlaced necklace can be seen with four droplets or tilab[c] at the ends. These tilab are made up of ever-smaller tilabs. There is a loltun[d] at the center of the figure. The halo around the central confined figure is also a feature that reappears again and again, as may be seen in the last inset of Fig. 7.

[b]ek-chaneb — star with four spikes in Mayan language.
[c]tilab — arrow in tseltal, one of the Mayan languages still spoken in southern Mexico.
[d]loltun — stone flower.

5. CONCLUSIONS

The quadratic iteration in 3D real scator space exhibits a rich boundary structure with complex escape velocity surrounding patterns. The hyperbolic numbers square bound set is obtained when real scator numbers are constrained to only two nonvanishing components.

Self-similar small copies of the larger bound set are obtained in the scalar (real) axis located at the same positions and relative sizes of the small M-set copies found on the real axis for the complex Mandelbrot set. Attractive periodic points are obtained when the quadratic function composition $R(R(R(z)))\cdots = R^n(z)$ returns the original argument $R^n(z_0) = z_0$. In the real axis, they are obtained from the real roots of the polynomials $z = 0$, $z^2+z = 0$, for a 1 period cycle; $(z^2+z)^2+z = 0$, for a 2 period cycle; $((z^2+z)^2+z)^2+z = 0$, for a 3 period cycle, etc. Remember that $\mathbb{R}$ is also a subset of the $1+m$, dimensional real scator set. Thus these roots, are also roots of the $1+2$ dimensional scator set. Recall that the logistic map exhibits a one to one correspondence with the M-set on the real axis. The Mandelbrot period doubling points coincide with the bifurcation points of the Verhulst process. The $\mathbf{c2i0}\mathbb{E}_+^{1+2}$ set exhibits this same one to one correspondence with the bifurcation diagram of the logistic map. As we have shown, it suffices to lift the second hypercomplex axis by 10^{-20} to reveal this structure. It is known that there are an infinite number of real polynomials' roots on this axis that come from the nth cycle periods. These periodic points have a basin of attraction. Furthermore, between -2 and the MF point, each of them exhibit self-similar copies of the larger set. For the quadratic iteration with real scators, there seem to be basins of attraction around the attractive periodic points in the scalar axis. These basins are observed in the s, x plane as shown in Fig. 3, also in the s, y plane (that is identical to the s, x plane) and the x, y plane as seen from Fig. 7. Thus, this real scator fractal set exhibits basins of attraction in a 3D space. Moreover, these small copies are self-similar 3D copies of the larger 3D bound set.

Many questions open up regarding these new fractal structures. So far, we have found no evidence of self-similar structures lying outside the scalar axis. Whether they exist is an open problem. Little has been mentioned regarding the Julia sets produced with real scator numbers $\mathbf{c2i}(c_s; c_x, c_y)\mathbb{E}_+^{1+2}(s; x, y)$ and its relationship with the $\mathbf{c2i0}\mathbb{E}_+^{1+2}(s; x, y)$ set. This issue will be undertaken in a forthcoming communication. The $\mathbf{c2i0}\mathbb{E}_+^{1+2}(s; x, y)$ set is much more difficult to explore than the complex M-set since it involves a 3D structure. 2D renderings can be made not only in planes with one constant component (as have been shown here) but also in inclined planes and even in nonplanar surfaces. Magnifications of different regions of the $\mathbf{c2i0}\mathbb{E}_+^{1+2}(s; x, y)$ set reveal extraordinary structures that we have only glimpsed at in an unsystematic fashion. 2D movies should prove useful to visualize the intricacies of the set.[12] 3D renderings should also turn out to be very useful to visualize the nature of these confined quadratic iteration real scator sets. We have produced some preliminary images using a 3D rendering program[11] as the one reproduced in Fig. 8. The 3D self-similar smaller set located around $(-1.75, 0, 0)$ is clearly visible. The two diamond shapes at the planes where one of the hypercomplex components is zero are also reckoned as well as the squeezing around the $s = 0$ plane on the far right. The various layers and the way they coalesce are an ode to mathematical enchantment.

ACKNOWLEDGMENTS

I dedicate this manuscript to the memory of Prof. Alonso Fernández-González, pioneer in crystal growth in Mexico and lifelong sculptor.

REFERENCES

1. P. Senn, The Mandelbrot set for binary numbers, *Am. J. Phys.* **58**(10) (1990) 1018.
2. W. Metzler, The "mystery" of the quadratic Mandelbrot set, *Am. J. Phys.* **62**(9) (1994) 813–814.
3. R. Artzy, Dynamics of quadratic functions in cycle planes, *J. Geometry* **44** (1992) 26–32.
4. D. G. Pavlov, M. S. Panchelyuga and V. A. Panchelyuga, About shape of Julia set at zero parameter on double numbers plane, *Hypercomplex Numbers in Geometry Phys.* **6** (2009) 146–151.
5. D. G. Pavlov, M. S. Panchelyuga, V. A. Malykhin and V. A. Panchelyuga, On fractality of Mandelbrot and Julia sets on double-numbers plane, *Hypercomplex Numbers in Geometry Phys.* **6** (2009) 135–145.
6. A. Douady, *Julia Sets and the Mandelbrot Set* (Springer-Verlag, 1986).
7. M. Fernández-Guasti and F. Zaldívar, A hyperbolic non distributive algebra in $1+2$ dimensions, *Adv. Appl. Clifford Algebras* **23**(3) (2013) 639–653.

8. M. Fernández-Guasti, Alternative realization for the composition of relativistic velocities, in *Optics and Photonics 2011*, Vol. 8121 The Nature of Light: What are Photons? IV (SPIE, 2011), pp. 812108–812111.
9. M. Fernández-Guasti, Lagrange's identity obtained from product identity, *Int. Math. Forum* **7**(52) (2012) 2555–2559.
10. B. B. Mandelbrot, *Fractals and Chaos: The Mandelbrot Set and Beyond* (Springer, 2004).
11. P. Willenius, Gestaltlupe, Available at https://github.com/trafassel/Gestaltlupe (2012).
12. M. Fernandez-Guasti, Available at http://luz.izt.uam.mx/gallery/c2i0ER2s,x,y2.gif 2012.